Journal of Visualization, Vol. 1, No. 3 (1999) 261-269

A Study of Pulsatile Jet Discharged from Pipe End

Endo, M.*[1] and Iwamoto, J.*[2]

*1 Tokyo Metropolitan College of Technology, Tokyo 140-0011, Japan.
*2 Tokyo Denki University, Tokyo 101-0054, Japan.

Received 30 July 1998.
Revised 2 November 1998.

***Abstract*:** Noise is generated from a flow field upstream of a shock wave periodically discharged from a pipe end. A vortex ring and an underexpanded jet are periodically formed and diffused downstream. To clarify the mechanism of the noise generation, the flow field was experimentally and numerically studied. The flow field was visualized mainly by the schlieren method and the sound pressure of the noise was measured. The pulsatile flow through the pipe was numerically simulated by Random-Choice Method and using these results as the boundary condition, the pulsatile jet was simulated by TVD scheme. As a result, a good qualitative agreement was found between the flow field obtained by the calculations and that by the experiments. Furthermore, a relation between the behaviour of the vortex ring and the generation of the noise was discussed.

***Keywords*:** simulation, pulsatile jet, noise generation, TVD scheme, Random-Choice Method

***Nomenclature*:**

e	total energy per unit mass
F	frictional force per unit mass
h	enthalpy
n	rotational speed of the rotary valve
p	pressure
Q	heat transfer per unit volume
r	internal radius of pipe
t	time
t_d	time measured from the instant when the shock wave reaches the end of the pipe
u	velocity for x-direction
v	velocity for y-direction
x	axial distance
y	radial distance
γ	ratio of specific heats
ρ	density
κ	heat conductivity
μ	viscosity
τ	period of one cycle of the rotary valve, or shear stress

1. Introduction

It is well known that behaviour of pressure waves, in particular, shock waves in exhaust pipes of a reciprocating internal combustion engine is closely related to its performance (Endo and Iwamoto, 1991). Compression wave generated at the exhaust port coalesces into shock wave as it propagates through the exhaust pipe, and reflects at some pipe elements so that a complicated flow field with shock waves results throughout the pipe.

Recently, the behaviour of the shock waves discharged into the atmosphere from the pipe end has attracted special interest because it is said to be one of the main causes of the exhaust noise (Takayama et al., 1989; Futagami and Iwamoto, 1996). In the flow field upstream of the discharged shock wave a vortex ring and an underexpanded jet are formed. Subsequently, the flow field develops, and the vortex ring and the underexpanded jet are diffused as they move downstream. This flow pattern repeats itself periodically. Noise is generated from such a flow field and the study of the noise generation has been done so far elsewhere. However, the mechanism for the noise generation has not been fully clarified yet.

In the present paper the flow field was experimentally and numerically studied and the relation between the behaviour of the vortex ring and the noise generation was discussed.

2. Experimental Considerations

A schematic view of an apparatus is shown in Fig. 1. Compressed air is supplied into the high pressure chamber. The air flows into a 1 m long straight pipe, whose internal diameter is 13 mm, through the rotary valve so that a pulsatile flow can be generated and the pulsatile jet is discharged into the atmosphere, or the experiment room.

Nine stations are located along the pipe for measurement of pressure histories using pressure transducers of a semi-conductor type. The distances between neighboring stations are 100 mm. The area change of the rotary valve is designed to be equal to that of an exhaust port of a typical four cycle internal combustion engine. The pressure in the high pressure chamber is kept at 4 bar although the pressure in the engine cylinder undergoes cyclic change by reciprocating motion of the pistons. This pressure is selected because the pressure in the cylinders at time of the valve opening is generally 4 bar and the pressure wave generated at this time characterizes the flow field. The volume of the experiment room, into which the pulsatile jet is discharged, is so large (W: 2400 mm × D: 2800 mm × H: 2100 mm), as shown in Fig. 2, that the pressure rise is negligible. The walls of the room are made of four layers; the glass wool, air layer, plasterboard and *tatami* mats for the purpose of measuring the exhaust noise. The noise is measured at some stations in the room using a condenser microphone. The flow field downstream of the pipe end is visualized by the schlieren method and the shadowgraph method.

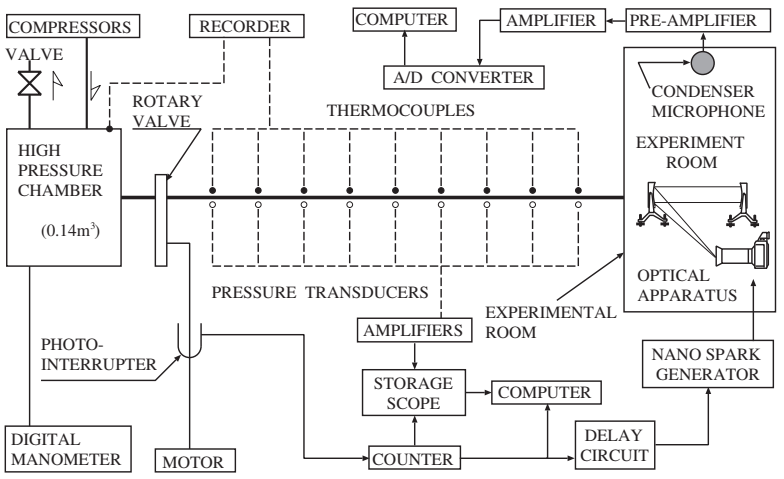

Fig. 1. Schematic view of apparatus.

3. Experimental Results

When the rotary valve opens, compression wave is generated and it propagates downstream through the pipe. A part of this compression wave coalesces into a shock wave, and then the shock wave is discharged into the atmosphere. The shock wave Mach number differs with the rotational speeds of the rotary valve. In the present experiment, however, the shock Mach number at the pipe end is in the range between 1.0 to 1.2. Unlike the shock in the shock tube, where the pressure behind the shock remains constant for a certain duration, in the present experiment the shock wave is followed by compression wave. Thus the pressure at the pipe exit continues to rise after the shock passes through it until the rarefaction wave reaches the pipe end.

The pressure change at a certain position outside the pipe takes a spike-shaped profile due to the discharged shock and the rarefaction wave generated at the edge of the pipe end which follows the shock. It is pointed out that noise is generated from a pipe end under this mechanism (Yasunobu et al., 1996). Figure 3 shows sound pressure histories at n = 3000 rpm at the station 1 m downstream of the pipe end along the line which lies 30 ° outward from the extension of the pipe as shown in Fig. 2. The ordinate is the sound pressure p_s in Pa and the abscissa is the time nondimensionalized by the period of one cycle of the area change of the rotary valve τ. As shown in the figure, the spike-shaped profile appears at the nondimensional times t/τ = 0.55 and 1.55. The sound pressure wave having broad-band frequency follows the spike-shaped wave, and it consists of mainly two kinds of pressure wave; one has low frequency and its amplitude decays as time proceeds and the other is of high frequency. That is, the high frequency pressure wave is superimposed on the low one.

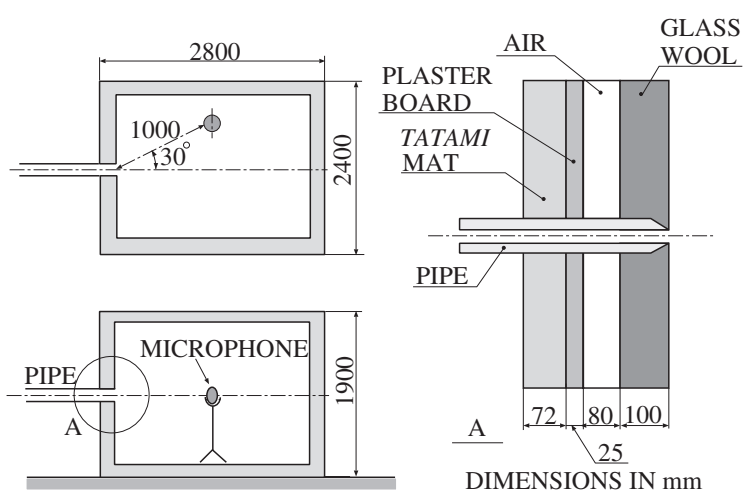

Fig. 2. Experiment room.

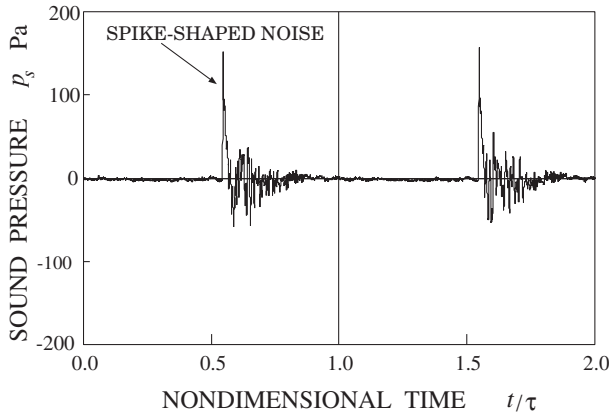

Fig .3. Sound pressure history.

Figure 4 shows a sequence of the flow pattern downstream of the pipe end. In Figs. 4(a) to 4(d), the flow pattern is visualized by means of the schlieren method at the rotational speed of the rotary valve, n = 3000 rpm. The shadowgram taken at n = 3600 rpm is shown in Fig. 4(e). In the schlieren method, the knife edge is placed normal to the flow direction. t_d is the time measured from the moment when the shock wave arrives at the pipe end. However, the time includes the error of about 0.01 ms caused by the delay circuit.

The discharged shock wave diffracts at the edge of the pipe end and then a vortex ring is generated as seen in Fig. 4(a). A region where the density is not uniform is found in the flow field downstream of the shock wave. It is caused by the jet generated in the previous cycle since the jet is periodically formed and diffused as mentioned above. From the time t_d = 0.03 ms a flat part of the shock wave becomes smaller and the size of the vortex becomes larger as time passes. At t_d = 0.11 ms the shock wave becomes almost spherical and the jet from the pipe end becomes underexpanded upstream of the vortex ring. In the upstream side of the vortex ring, the pattern of the density distribution is found to be rolled-up. In the flow field between the vortex ring and the shock wave some

pressure waves appear. They are almost spherical like that of the shock wave and considered to be generated successively. Their sources can be considered as a circular plane or a ring judging from the shape of the waves. These pressure waves are considered to be the source of the noise following spike-shaped wave as shown in Fig. 3. At $t_d = 0.20$ ms the flow field develops further. The vortex ring becomes much larger and the flow field of the upstream side of the vortex ring is further rolling. This is considered to be caused by the interaction of the vortex ring with the underexpanded jet. Additionally, a weak pressure wave which stretches into the core of the vortex ring is found. Each wave front is curved and the wave length of the outer side is greater than that of the inner side. Figure 4(e) shows the shadowgram at $t_d = 0.22$ ms. In the figure, only the strong waves can be seen and the shock wave is found to be formed in the vortex ring.

Thus, the vortex ring is induced by the discharged shock wave downstream of the pipe end. The flow field develops and the underexpanded jet is formed in the flow field between the pipe end and the vortex ring. In this process, the shock wave appears in the vortex ring and the pressure wave is generated in the vicinity of the vortex core. The almost spherical pressure waves follow the discharged shock wave and they are successively generated. Consequently, these pressure waves are considered to be the source of the noise following the spike-like wave as shown in Fig. 3.

4. Numerical Scheme

The numerical analysis was made by the coupling of two procedures; the pulsatile flow through the pipe was simulated by a one-dimensional scheme known as a RCM (Endo and Iwamoto, 1992) and, using these results as the boundary condition, the pulsatile jet with the vortex ring was simulated by a TVD scheme (Sakakibara and Iwamoto, 1995) under the assumption of axially-symmetric flow

4.1 Random-choice Method

One-dimensional, unsteady and compressible flow field through the pipe of the constantcross-sectional area is governed by the following equations:

$$\rho_t + (\rho u)_x = 0 \tag{1}$$

$$(\rho u)_t + (\rho u^2 + p)_x = -\rho F \tag{2}$$

$$(\rho e)_t + (\rho u e + u p)_x = Q \tag{3}$$

$$e = \frac{1}{\gamma - 1}\frac{p}{\rho} + \frac{u^2}{2} \tag{4}$$

where p, ρ, u, t, x, γ and e are the pressure, density, flow velocity, time, distance, ratio of the specific heats and total energy per unit mass, respectively. F is the frictional force per unit mass and Q is the heat transfer per unit volume.The subscripts t and x represent the partial derivatives with respect to the time and the distance, respectively.The set of equations is numerically solved using the RCM.

In the present calculation, the flow field is divided into 200 cells along 1 m long pipe. As the initial conditions, the flow states over each cell, i.e. at each grid point, are assumed to be under atmospheric conditions and the flow velocity to be zero. The flow states which change with time at the position 100 mm upstream of the pipe end are obtained using the RCM during 20 periods of the cycle of the valve opening area change. They are ensemble-averaged and becomes available as the boundary conditions for solving the flow field downstream of the pipe end using the TVD scheme.

4.2 TVD Scheme

Two-dimensional, axially-symmetric and compressible flow field is governed by the following equations:

$$U_t + F_x + G_y = H \tag{5}$$

where the subscripts t, x and y represent the partial derivatives and,

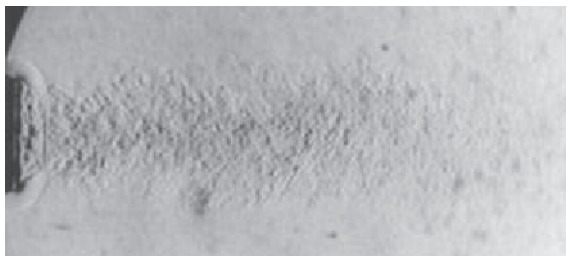

(a) t_d = 0.01 ms, n = 3000 rpm

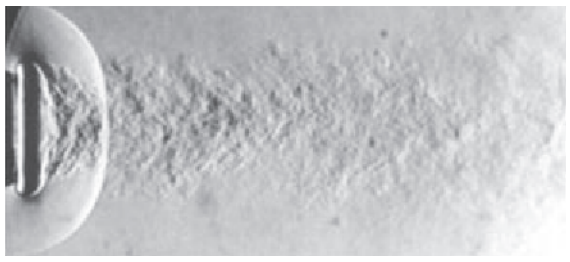

(a) t_d = 0.03 ms, n = 3000 rpm

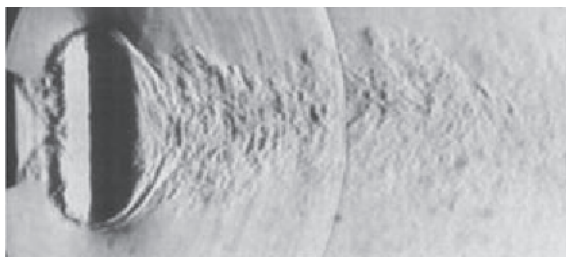

(b) t_d = 0.11 ms, n = 3000 rpm

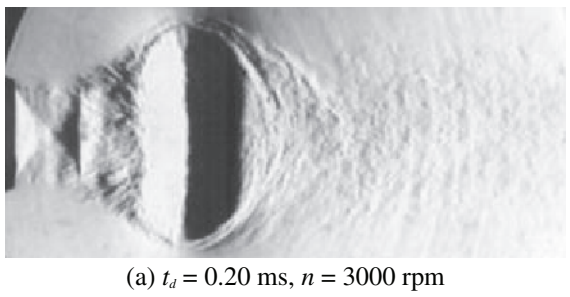

(a) t_d = 0.20 ms, n = 3000 rpm

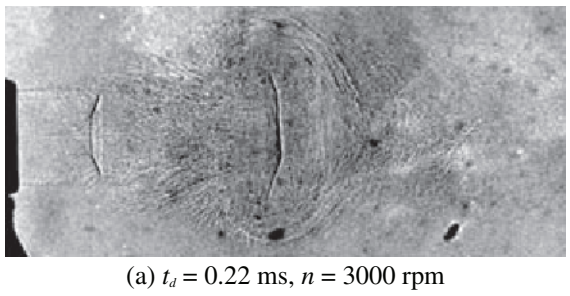

(a) t_d = 0.22 ms, n = 3000 rpm

Fig .4. Visualized flow pattern.

$$\boldsymbol{U} = \begin{bmatrix} \rho \\ \rho u \\ \rho v \\ \rho e \end{bmatrix} \tag{6}$$

$$\boldsymbol{F} = \begin{bmatrix} \rho u \\ p + \rho u^2 + \tau_{xx} \\ \rho uv + \tau_{xy} \\ \rho uh + \tau_{xx}u + \tau_{xy}v - \kappa \dfrac{\partial T}{\partial x} \end{bmatrix} \tag{7}$$

$$\boldsymbol{G} = \begin{bmatrix} \rho v \\ \rho uv + \tau_{xy} \\ p + \rho v^2 + \tau_{yy} \\ \rho vh + \tau_{yy}v + \tau_{xy}u - \kappa \dfrac{\partial T}{\partial y} \end{bmatrix} \tag{8}$$

$$\boldsymbol{H} = \begin{bmatrix} -\rho v / y \\ -\tau_{xy}/y - \rho uv/y \\ -\tau_{yy}/y - \rho v^2/y \\ -\left(\tau_{yy}v + \tau_{xy}u - \kappa \dfrac{\partial T}{\partial y} \right) / y - \rho vh/y \end{bmatrix} \tag{9}$$

where p, ρ, u and v are the pressure, density and velocities for x and y directions, respectively. x is in the flow direction and y the radial direction. The total energy per unit mass e and the enthalpy h are given as follows:

$$e = \frac{1}{\gamma - 1} \frac{p}{\rho} + \frac{u^2 + v^2}{2} \tag{10}$$

$$h = e + \frac{p}{\rho} \tag{11}$$

The shear stresses τ_{xx}, τ_{yy}, and τ_{xy} are given using the viscosity μ and the heat conductivity κ.

The governing equations are solved by using the symmetric TVD scheme by Yee with β limiter function, its accuracy being 2nd-order both in space and time. As shown in Fig. 5, the computational region covers the part of the flow field through the pipe as well as the flow field downstream of the pipe end. The length of the pipe covered by the computational region is $15.3r$ (100 mm) and the flow field downstream of the pipe end $15.3r \times 15.3r$, where r is internal radius of the pipe equal to 6.5 mm. The number of nodes for x-direction is 824 and that for y is 412. These nodes are coagulated toward the center axis and the baffle plate of the pipe end.

The boundary conditions at the position $15.3r$ in the pipe upstream of the pipe end are given using the numerical results by the RCM. The boundaries at the wall of the pipe and the baffle plate are reflective and the non-slip condition is assumed there. The boundary condition that the space derivatives of the flow variables are equal to zero is given at the upper side of the computational region and also at the downstream end. The atmospheric states and zero velocity of the flow are given throughout the computational region as the initial conditions.

5. Numerical Results

In Fig. 6 the computational results at n = 3000 rpm are shown at the different times ranging from t_d = 0.02 ms to t_d = 0.19 ms in the first cycle starting with the initial conditions. t_d = 0.00 ms means that the discharged shock wave stands exactly at the pipe end. In these figures the density contours of the flow field ($15r$ to $25r$ for x-direction and 0 to $3.5r$ for y-direction) are shown in the upper half and the pressure contours in the lower half. The different colors show the different levels of pressures or densities nondimensionalized by the atmospheric state; the red lines show the high values and the blues ones low as in the color indicator.

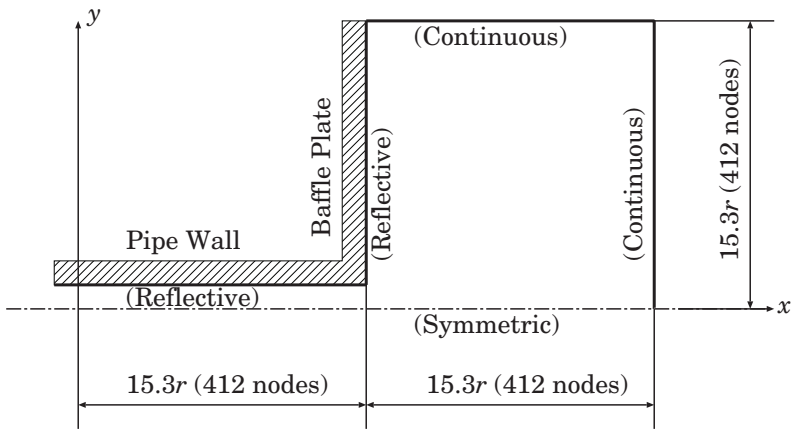

Fig .5. Computational region.

At t_d = 0.02 ms, the wave front of the discharged shock, which is flat over the cross section of the pipe at t_d = 0.00 ms, becomes almost spherical. The jet boundary starts to form and the vortex ring is generated at the pipe end.The size of the vortex is small and the diameter of the vortex ring, i.e. that of the circle of the vortex core, is greater than that of the pipe. Thus, the jet is considered to flow smoothly into the atmosphere. At t_d = 0.10 ms, the shock wave propagates downstream and decays. Downstream of the vortex ring, the contact surface looks like a dome in its shape.The size of the vortex becomes larger and so, the jet converges and its boundary rolls up in the vortex ring. Then, a shock wave occurs at the jet boundary in the vortex ring. This is considered to be caused by an effect which can be observed in a Laval nozzle. In other words, the relative velocity of the jet just upstream of the vortex ring to the vortex ring is subsonic. The cross-sectional area of the jet decreases first, and then increases along the jet axis in the flow direction. Thus, the relative velocity reaches the sonic velocity at the throat of the jet in the vortex ring and the supersonic region appears in the vicinity of the jet boundary where the shock wave is generated. The underexpanded jet develops between the pipe end and the vortex ring. The intercepted oblique shock wave is formed in the jet.

At t_d= 0.12 ms, the jet at the upstream side of the vortex ring is expanded, i.e. jet boundary meanders, so that a small vortex is generated at the jet boundary. This small vortex upstream of the large one induced by the shock wave is considered to be visualized by the schlieren method as non-uniform density distribution upstream of the large vortex as shown in Fig. 4(c). The shape of the large vortex is no longer circular and is now elliptical because of the sinuous jet boundary. The shock wave generated at the jet boundary spreads throughout the vortex ring, resulting in the normal shock wave. At t_d = 0.15 ms, a new vortex ring is formed at the jet boundary in the same manner as that at t_d = 0.12 ms. This small vortex is sucked in by the large vortex ring and approaches the normal shock wave. The shape of the large vortex is further distorted and the pressure wave stretching into the vortex core is generated. These pressure waves are curved in the direction of the vortex rotation as shown in Fig. 6(d). They are visualized in Fig. 4(d). At t_d= 0.17 ms, the approaching vortex ring breaks through the shock wave and then, a new pressure wave is generated downstream of the dome-shaped contact surface which surrounds the vortex ring. Subsequently, the small vortex ring is captured by the large one at t_d = 0.19 ms and a complicated flow field is formed. The newly generated pressure wave propagates downstream and follows the discharged shock wave as its shape changes into a spherical one. Additionally, the weak waves are formed in the flow field between the new pressure wave and the dome-shaped contact surface. These are considered to be caused by the interaction of the small vortex with the large one. The small vortices upstream of the large one are visualized as the rolling and stretched density wave shown in Fig. 4(d). The pressure waves induced by such interaction are considered to correspond to the pressure wave visualized by the schlieren method as shown in Figs.4(c) and (d).

Thus, the small vortices are generated at the jet boundary as the jet is expanded. Some of them interact with the shock wave in the large vortex ring, resulting in new pressure waves emanating from the large vortex ring. They are almost periodically generated, though the numerical results are not shown for the time later than t_d = 0.19 ms in Fig. 6. Furthermore, it is considered that the vortex associated with the normal shock wave diffuses and decays as the small vortex strikes the shock wave. Consequently, the sound pressure wave following the spike-shaped wave in Fig.3 is introduced in this procedure. The low frequency wave is considered to be caused by the pressure wave induced by the interaction.

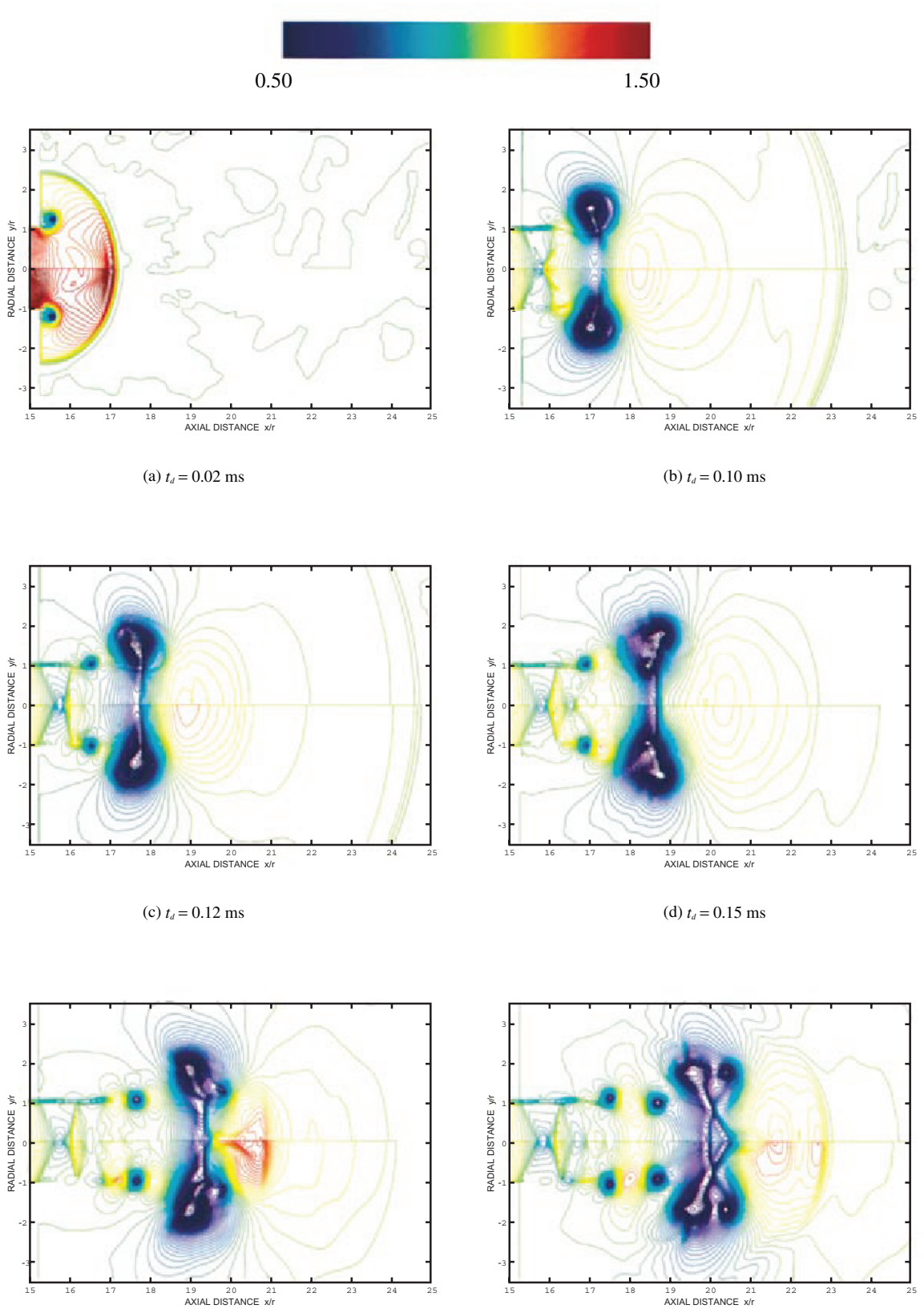

(a) $t_d = 0.02$ ms

(b) $t_d = 0.10$ ms

(c) $t_d = 0.12$ ms

(d) $t_d = 0.15$ ms

(e) $t_d = 0.17$ ms

(f) $t_d = 0.19$ ms

Fig .6. Density and pressure contours.

6. Conclusions

In order to analyze the mechanism of the noise generation from the pulsatile flow field downstream of the exhaust pipe end, experimental and numerical studies are carried out. These results are discussed and compared with each other. As a result, the following conclusions can be drawn:

(1) The source of the noise, in addition to that due to the shock wave discharged from the pipe end, is considered to exist as shown by the measured sound pressure.
(2) The flow pattern obtained by the calculations qualitatively agrees well with that given by the experiments.
(3) In the flow field between the vortex ring and the discharged shock wave, the spherical pressure wave front is experimentally and numerically visualized.
(4) The small vortex is found to be generated at the jet boundary due to interaction of the jet boundary with the vortex ring as suggested by the computational results.
(5) A pressure wave is found to be generated by the small vortex ring hitting the shock wave in the vortex ring from the computational results.
(6) The pressure wave induced by the interaction of the small vortex with the large one is considered to be the source of the noise.
(7) The behaviour of the vortex ring and jet boundary is considered to be related to the noise generation.

Acknowledgment

The experimental data described above were supplied from the experiments by Messrs. T. Furuya and Y. Morita. The authors wish to record their thanks to them for the use of their experimental results.

References

Endo, M. and Iwamoto, J., The Influence of Wave Action on Mass Flow Rate through Pipes, SAE Paper, 911724 (1991).

Takayama, K. et al., Shock Wave Development and Propagation in Automobile Exhaust Systems, SAE Transactions, 880082 (1989), 4.66-4.72.

Futagami, Y. and Iwamoto, J., A Study on the Relation Between Pulsating Flow and the Noise, SAE Paper, 961822 (1996).

Yasunobu, T. et al., Numerical Analysis of Flow Caused by Emission of Compression Wave from Open End of Circular Tube, Trans. JSAE (B), 62-596 (1996), 1313-1320 (in Japanese).

Endo, M. and Iwamoto, J., A Numerical Study of Pulsating Flow in a Duct with a Junction, SAE Transactions, 911783 (1992), 1482-1487.

Sakakibara, Y. and Iwamoto, J., Numerical Study of Self-Excited Oscillation of Supersonic Jet Impinging on Plate, Proceedings o f the International Conference on Computational Engineering Science, (1995), 1059-1064.

Authors' Profiles

Masaki Endo: He received his BSc (Eng), MSc (Eng) and Ph.D. (Eng) degree in Mechanical engineering in 1988, 1990 and 1993 from Tokyo Denki University, re-spectively. He was supervised in Pulsating Flow in Pipe by Prof. J.Iwamoto, or co-author. He took up his position as assistant at Tokyo Metropolitan College of Tech-nology in 1993. In 1996 he was promoted to assistant professor of mechanical engineering at Tokyo Metropolitan College of Tech-nology. His research interests have been expanded to phenomena in unsteady high speed flow field with shock wave.
Assistant Professor of Mechanical Engineering, Tokyo Metropolitan College of Technology.

Junjiro Iwamoto: He received his BSc (Eng) and MSc (Eng) degree in Mechanical engineering in 1962 and 1966, respectively, from College of Engineering, Keio University, and his Ph.D. in High-Speed Oscillatory Flow in 1970 from Keio University. He worked as an engineer for Toyota Motor Company from 1962 to 1964. He took up his position as assistant professor at Tokyo Denki Uni-versity in 1969. In 1980 he was promoted to professor of mecha-nical engineering at Tokyo Denki University. His research interests include high-speed flow, shock dynamics and pulsating flow.
Professor of Mechanical Engi-neering, Tokyo Denki University.